Numerical and Experimental Study of Various Interior Source Identification Methods with Circular Microphone Arrays

Iman Khatami *[1] **and Alain Berry** †[2]

[1]Departement of Mechanical Engineering, Chabahar Maritime University, Iran
[2]Departement of Mechanical Engineering, Universite de Sherbrooke, Canada

Résumé

Cette étude évalue plusieurs méthodes d'identification de sources basées sur des antennes microphoniques circulaires, dans le cas de sources intérieures au réseau circulaire. Plusieurs techniques sont comparées, dont la formation de voie classique (CB), les méthodes inverses régularisées (régulariation de Tikhonov), la formation de voie inverse généralisée L1 (L1-GIB), les méthodes de déconvolution CLEAN-PSF, CLEAN-SC, ainsi que des méthodes plus récentes utilisant une régularisation par formation de voie (BFR). De plus, nous proposons une nouvelle méthode (CLEAN-BFR), qui combine les approches itératives de CLEAN-SC et BFR. Pour mettre en évidence les avantages et désavantages de ces méthodes, plusieurs exemples d'application numériques et expérimentaux sont discutés. Lorsque des sources multiples doivent être identifiées, les résultats montrent que la méthode à choisir dépend de la corrélation, de la directivité et du niveau relatif des sources.

Mots clefs : méthodes d'identification de sources, antenne microphonique circulaire, formation de voie, méthodes inverse, déconvolution.

Abstract

This study addresses an assessment of some sound identification methods using circular microphone arrays for sources interior to the array circle. Various techniques are compared, including classical beamforming (CB), regularized inverse methods (Tikhonov regularization), L1- generalized inverse beamforming (L1-GIB), deconvolution methods CLEAN-PSF, CLEAN-SC, as well as more recent inverse methods using beamforming regularization (BFR). Furthermore, a new method (CLEAN-BFR) combining the iterative concepts of CLEAN-SC and BFR has been proposed. To highlight the advantages and disadvantages of these methods, several numerical and experimental application examples are discussed. When multiple sources are searched, the results show that the method of choice depends on the correlation, directivity and relative level of the sources.

Keywords: noise identification methods, circular microphone array, beamforming, inverse method, deconvolution

1 Introduction

The disturbing effects of noise on people motivate researchers to identify and maintain noise under a certain level. Extensive work has been done to develop methods to identify, locate and quantify various types of noise sources in many different contexts. This work is mainly concerned with the identification of aircraft engine inlet and exhaust noise. Aircraft engines are subject to static, ground tests for noise level certification, in which engine noise is measured externally in different directions by a circular microphonic antenna placed in the far field of the engine (to see more details refer to [1]). The possibility of using these measurements to discriminate and quantify engine inlet and exhaust noise has not yet been studied.

Researchers have investigated a number of algorithms to detect noise sources and have attempted to increase the spatial resolution and accuracy of source strength maps by removing or filtering side lobes from the map. These algorithms are usually based on Phased Array Beamforming [2-4] or Inverse Methods [3, 5, 6]. Beamforming is a very common method that successfully identifies the sound source even when the source intensity is well below the background noise level. Sarradj [7] proposed a subspace-based beamforming method focused on signal subspace and leading to a computationally efficient estimation of the source strength and location, with monopole or multipole radiation patterns [8]. Bravo et al [3] tested beamforming and inverse methods for the localization of in-duct sources.

Michel et al [5] compared inverse methods with conventional beamforming for the source distribution along the axis of a high bypass ratio aero-engine.

Recently, a few hybrid methods using subspace analysis and beamforming have been proposed, such as inverse methods with a regularization based on an initial beamforming solution [9-12], the Multiple Signal Classification(MUSIC) [13] and the application of a subspace invariance approach (ESPRIT) [14]. In MUSIC and ESPRIT, the useful signal and measurement noise components are split into identified subspaces to minimize the effect of noise. This differs from "deconvolution" approaches in which the aim is to attenuate the effect of the point-spread function in the beamforming map and consequently refine the localization of the sources.

* iman.khatani81@gmail.com
† alain.berry@usherbrooke.ca

The main deconvolution approaches are CLEAN [15] and DAMAS [16, 17]. Susuki [18, 19] developed the Generalized Inverse Beamforming (GIB) to resolve coherent or incoherent, distributed or compact aerodynamic sound sources using an eigenmode decomposition of the cross-spectral matrix of microphone signals.

In this paper, the applicability of five sound identification methods as well as two novel methods, BRF and CLEAN-BRF, is evaluated in the context of acoustic source separation using a circular microphone array configuration.

The remainder of this paper is organized as follows: in section 2, the source identification algorithms are briefly explained. In section 3, the applicability of the proposed algorithms is investigated for various simulated sound sources. In section 4, the simulation study is validated through experiments using a circular microphone array.

2   Source Identification Methods

2.1   Beamforming

Beamforming is a technique that separates desired signals from noise. In the output of beamforming, the desired signals added coherently whereas noise is added incoherently.

We assume here that the identified acoustic sources are represented by a set of L candidate point sources distributed over a target grid domain and that there are M microphones to measure the magnitude of the sound sources. The sound pressure field of a point source at location $\mathbf{r}$ is given by [20]:

$$p_m(\mathbf{r}, \omega) = \frac{q_0 \, e^{-jk|\mathbf{r}-r_m|}}{|\mathbf{r} - r_m|},\tag{1}$$

where q_0 is the source strength, $\mathbf{r}_m$ ($m = 1,2,3 \dots M$) is the location of the mth microphone, k is the wavenumber and ω is the angular frequency. The normalized beamforming output is given by [21]:

$$B(\mathbf{r}, \omega) = \alpha \sum_{m=1}^{M} g_m{}^* p_m(\mathbf{r}, \omega) = \alpha \mathbf{g}^{\mathrm{H}} \mathbf{p}\tag{2}$$

where α is the weight vector normalization coefficient, $g_m = e^{-jk|\mathbf{r}-r_m|}/|\mathbf{r} - r_m|$ is the mth component of the $M \times 1$ steering vector $\mathbf{g}$, $*$ is the complex conjugate and $^{\mathrm{H}}$ is the Hermitian transpose. This vector consists of complex pressure amplitudes emanated by a unit monopole point source in $\mathbf{r}$. The average power of equation 2 is given by:

$$\begin{aligned}A(\mathbf{r}, \omega) = |B(\mathbf{r}, \omega)|^2 &= \alpha^2 \mathbf{g}^{\mathrm{H}} \mathbf{p}\mathbf{p}^{\mathrm{H}} \mathbf{g} \\ &= \alpha^2 \mathbf{g}^{\mathrm{H}} \mathbf{C} \mathbf{g}\end{aligned}\tag{3}$$

where $\mathbf{C} = \mathbf{p}\mathbf{p}^{\mathrm{H}}$ is the $M \times M$ Cross Spectral Matrix (CSM). The appropriate normalization coefficient α can be derived in the following way. If a set of L point sources is considered at locations $\mathbf{y}_l$, the model for the pressure ($\mathbf{p}$) at microphone positions can be written by [21]:

$$\mathbf{p} = \sum_{l=1}^{L} q_l \, \mathbf{g}_l\tag{4}$$

where q_l is the strength of source at point $\mathbf{y}_l$ and $\mathbf{g}_l$ is the the $M \times 1$ vector of components $g_{ml} = e^{-jk|\mathbf{r}_l-r_m|}/|\mathbf{r}_l - r_m|$. Substituting equation 4 into equation 3 for a single source l and for $\mathbf{r} = \mathbf{y}_l$ gives:

$$A_{ll} = \alpha^2 q_l q_l{}^* \mathbf{g}_l{}^{\mathrm{H}} \mathbf{g}_l \mathbf{g}_l{}^{\mathrm{H}} \mathbf{g}_l \,.\tag{5}$$

Since it is requested that $q_l q_l{}^* = A_{ll}$, equation 5 can be written as:

$$A_{ll} = \alpha^2 A_{ll} \mathbf{g}_l{}^{\mathrm{H}} \mathbf{g}_l \mathbf{g}_l{}^{\mathrm{H}} \mathbf{g}_l \,.\tag{6}$$

Therefore, solving for α gives:

$$\alpha = \frac{1}{\sqrt{(\mathbf{g}_l{}^{\mathrm{H}} \mathbf{g}_l)^2}} = \frac{1}{\sqrt{\sum_{(m,n) \in S}|g_{ml}|^2 |g_{nl}|^2}}\tag{7}$$

where S is assumed to be a subset of all possibilities of (m,n)-combinations, and m and n are microphone indices. Defining the array weight vector by $\mathbf{W} = \alpha \mathbf{g}$, equation 3 can be rewritten [15]:

$$A = \mathbf{W}^{\mathrm{H}} \bar{\mathbf{C}} \, \mathbf{W} \,,\tag{8}$$

$\bar{\mathbf{C}}$ is the cross spectral matrix (CSM) of microphone signals where the diagonal of the matrix is removed. The diagonal removal eliminates the effect of uncorrelated measurement noise among microphone signals, which is therefore restricted to microphone auto-spectra.

The normalized beamforming delay-and-sum operation can also be written by

$$\mathbf{q}_{\mathrm{BF}} = \alpha \mathbf{G}^{\mathrm{H}} \mathbf{p}\tag{9}$$

where $\mathbf{q}_{\mathrm{BF}}$ is the $L \times 1$ beamformer output vector at the L candidate source locations and $\mathbf{G}$ is the $M \times L$ matrix of free-field Green's functions between the L point sources and M sound pressure measurement points. Therefore, the beamformer power output matrix is defined by

$$\mathbf{A} = \mathbf{q}_{\mathrm{BF}} \mathbf{q}_{\mathrm{BF}}{}^{\mathrm{H}} = \alpha^2 \mathbf{G}^{\mathrm{H}} \bar{\mathbf{C}} \mathbf{G} \,.\tag{10}$$

2.2   Inverse Method

For practical sound field identification based on inverse problem theory, the general inverse problem must be discretized in terms of the source description. We assume here again that the acoustic sources are represented by a set of L point sources and that there are M microphones. The matrix form of equation 4 which is the sampled direct radiation problem is written as

$$\mathbf{p} = \mathbf{G} \mathbf{q}\tag{11}$$

where $\mathbf{p}$ is the $M \times 1$ vector of complex sound pressure values at the microphone locations, $\mathbf{G}$ is the $M \times L$ vector matrix of free-field Green's functions between the L point sources and M sound pressure measurement points, $\mathbf{q}$ is the $L \times 1$ vector of unknown complex source strengths. In the inverse method, the 2-norm of the error between the reconstructed sound pressure $\mathbf{p}$ assuming a set of L point sources and the measured sound pressure $\mathbf{p}$ is minimized.

The problem is then to find the optimal q for the minimization problem

$$\mathbf{q}_{\mathrm{opt}} = \arg\min\{|\mathbf{p} - \mathbf{G}\mathbf{q}|^2\}.\tag{12}$$

Most of the time the inverse problem is ill-conditioned, implying that the solution $\mathbf{q}_{opt}$ is very sensitive to measurement noise and model uncertainty. To prevent this problem, Tikhonov regularization is used [6, 9]. Therefore, the regularized inverse problem is:

$$\mathbf{q}_{\text{opt}} = \text{argmin} \left\{ |\mathbf{p} - \mathbf{Gq}|^2 + \epsilon^2 |\mathbf{Lq}|^2 \right\} \qquad (13)$$

where ϵ is the regularization parameter and L is the discrete smoothing norm used to shape the regularization. In this work, the optimal regularization parameter is based on the well-known L-curve criterion [22].

The L-curve is a plot of the norm of the regularized solution versus the norm of the corresponding residual for all valid regularization parameters. The curve very often has an "L" shape and the corner of the L-curve balances the minimization of the residual norm ($\|\mathbf{Gq} - \mathbf{p}\|^2$) and the norm of $\|\mathbf{q}\|^2$. The solution of this minimization problem is:

$$\mathbf{q}_{\text{opt}} = (\mathbf{G}^H\mathbf{G} + \epsilon^2\mathbf{L})^{-1}\mathbf{G}^H\mathbf{p} \qquad (14)$$

The simplest form of Tikhonov regularization uses $\mathbf{L} = \mathbf{I}$ where $\mathbf{I}$ is the identity matrix therefore the a $L \times L$ source power matrix provided by the inverse solution is given by:

$$\mathbf{A} = \mathbf{q}_{\text{opt}}\mathbf{q}_{\text{opt}}^H = \\ (\mathbf{G}^H\mathbf{G} + \epsilon^2\mathbf{I})^{-1}\mathbf{G}^H\bar{\mathbf{C}}\,\mathbf{G}[\,(\mathbf{G}^H\mathbf{G} + \epsilon^2\mathbf{I})^{-1}]^H. \qquad (15)$$

2.3 Inverse Solution using Beamforming Regularization (BFR)

In this section, a novel method combining the iterative concepts of CLEAN-SC and BFR has been presented. The main idea behind the proposed regularization approach is to find a "best" smoothing norm L in our problem [9]. This can be performed by observing that part of the solution given by equation 14 involves the beamforming delay-and-sum operation

$$\mathbf{q}_{\text{BF}} = \mathbf{G}^H\mathbf{p} . \qquad (16)$$

Therefore, an application of the general Tikhonov regularization problem (equation 13) is to use the special case where the regularization matrix L is related to the beamforming output,

$$\mathbf{L} = [\text{diag}(|\mathbf{G}^H\mathbf{p}|/\|\mathbf{G}^H\mathbf{p}\|_\infty)]^{-1} \qquad (17)$$

where diag($|\mathbf{a}|$) indicates that the absolute value of the $1 \times L$ vector $\mathbf{a}$ is mapped on the main diagonal of a $L \times L$ matrix. The infinity norm of a vector $\mathbf{v}$ is denoted $\|\mathbf{v}\|_\infty$ and is defined as the maximum of the absolute values of its components. Note that the beamforming output $\mathbf{G}^H\mathbf{p}$ has been normalized by its infinity norm $\|\mathbf{G}^H\mathbf{p}\|_\infty$ to ensure that the regularization is normalized in terms of beamformer signal level. Thus, the minimization problem (equation 13) becomes:

$$\mathbf{q}_{\text{opt}} = \text{argmin} \left\{ |\mathbf{p} - \mathbf{Gq}|^2 + \\ \epsilon^2 |[\text{diag}(|\mathbf{G}^H\mathbf{p}|/\|\mathbf{G}^H\mathbf{p}\|_\infty)]^{-1}\mathbf{q}|^2 \right\}. \qquad (18)$$

Therefore, the inverse solution with such a regularization matrix favors source positions or directions for which classical beamforming yields a large output. The square diagonal matrix $[\text{diag}(|\mathbf{G}^H\mathbf{p}|/\|\mathbf{G}^H\mathbf{p}\|_\infty)^2]^{-1}$ is called the

beamforming regularization matrix. It is important to note that this approach involves a data-dependent regularization which somewhat differentiates this method from most classical regularization methods. The solution of the above minimization problem then becomes:

$$\mathbf{q}_{\text{BFR}} = (\mathbf{G}^H\mathbf{G} + \\ \epsilon^2[\text{diag}(|\mathbf{G}^H\mathbf{p}|/\|\mathbf{G}^H\mathbf{p}\|_\infty)^2]^{-1})^{-1}\,\mathbf{G}^H\mathbf{p} . \qquad (19)$$

As a consequence, the source power map of the BFR method is given by:

$$\mathbf{A} = \mathbf{W}_{\text{BFR}}{}^H\bar{\mathbf{C}}\mathbf{W}_{\text{BFR}} \qquad (20)$$

where $\mathbf{W}_{\text{BFR}} = (\mathbf{G}^H\mathbf{G} + \\ \epsilon^2[\text{diag}(|\mathbf{G}^H\mathbf{p}|/\|\mathbf{G}^H\mathbf{p}\|_\infty)^2]^{-1})^{-1}\,\mathbf{G}^H.$

2.4 L1-Generalized Inverse Beamforming (L1-GIB)

Similar to the beamforming method, pre-defined monopoles and dipoles are considered in L1-GIB to obtain the source distribution. The source distribution is solved as an L1 norm problem using Iteratively Re-weighted Least Squares (IRLS). The source detection problem is defined to be a minimization of the following L_p norm cost function [18, 19]:

$$J_p = \sum_i^{L_{\text{type}}L} |\mathbf{q}_i|^p + \vec{\lambda}\,(\mathbf{v}_i - \mathbf{Gq}_i), \qquad (21)$$

where $\mathbf{q}_i$ is a $L_{\text{type}}L \times 1$ vector that consists of complex source amplitudes for all source types and for all target domain grid points , L_{type} indicates the number of specified source types (monopoles, dipoles and possibly higher-order multipoles) and L is the number of grid points. Also, $\mathbf{v}_i$ are the eigenmodes, defined as the normalized $M \times 1$ eigenvectors of the cross-spectral matrix C, G is the $M \times L_{type}L$ propagation matrix from all sources to all microphones and $\vec{\lambda}$ is the Lagrange multiplier vector.

The minimization of equation 21 is solved using the IRLS method [23] which iteratively solves general L_p norm problems. Equation 21 can be written as

$$J_p = \sum \mathrm{w}_i^{-1}|\mathbf{q}_i|^2 + \vec{\lambda}(\mathbf{v}_i - \mathbf{Gq}_i) \qquad (22)$$

where $\mathrm{w}_i^{-1} = |\mathbf{q}_i|^{p-2}$. This function is iteratively minimized using a generalized iterative method as

$$\mathbf{q}_i{}^{(n+1)} = \mathbf{W}_i{}^{(n)}\mathbf{G}^H\big(\mathbf{G}\mathbf{W}_i{}^{(n)}\mathbf{G}^H + \epsilon\mathbf{I}\big)^{-1}\mathbf{v}_i , \qquad (23)$$

where $\mathbf{W}_i{}^{(n)}$ is the $(L_{\text{type}}L) \times (L_{\text{type}}L)$ diagonal matrix in which the diagonal component is given by $\mathrm{w}_i = |q_i|^{2-p}, q$ is a component of vector $\mathbf{q}$ and the superscript n is the iteration counter.

2.5 CLEAN-PSF

CLEAN-PSF (based on point speed function) is a deconvolution method that helps compensating for Point Spread Functions (PSF's) in source plots. This method attempts to substitute these PSF's with single points, or beams with narrow widths. The steps of CLEAN-PSF are as follows [15]:

- Obtaining the source plot using classical beamforming ("dirty map")
- Searching for the peak location in the dirty map
- Subtracting the appropriately scaled PSF from the dirty map
- Replacing the PSF by a clean beam
- This process is performed iteratively to detect all sources

In the first iteration ($i = 0$) $\overline{\mathbf{D}}^{(i)}$ is defined as the cross-spectral matrix with diagonal components removed $\overline{\mathbf{C}}$

$$\overline{\mathbf{D}}^{(i)} = \overline{\mathbf{D}}^{(0)} = \overline{\mathbf{C}} \tag{24}$$

Source powers $A_j^{(0)}$ using classical beamforming (which are components of $\mathbf{A}$ in equation 10 are given by:

$$A_j^{(0)} = \mathbf{W}_j^{\mathrm{H}}\overline{\mathbf{C}}\mathbf{W}_j = \mathbf{W}_j^{\mathrm{H}}\overline{\mathbf{D}}^0\mathbf{W}_j \tag{25}$$

where $\mathbf{W}_j$ is the weigth vector for the scan (or grid) point j. The next step ($i \geq 1$) is the detection of the grid location $\mathbf{y}_{max}$ for which the source power map is maximal and the amplitude of this peak ($A_{max}^{(i-1)}$) from the dirty map. Then, the contribution of the source associated with the peak power is subtracted from the dirty map. At this point, the PSF associated with the peak source is removed in the degraded source powers $A_j^{(i)}$. These degraded source powers are given by:

$$A_j^{(i)} = A_j^{(i-1)} - \mathbf{W}_j^{\mathrm{H}}\overline{\mathbf{G}}^{(i)}\mathbf{W}_j, \tag{26}$$

where $\overline{\mathbf{G}}^{(i)}$ is the CSM with the diagonal removed, obtained for the source in $\mathbf{y}_{max}$,

$$\mathbf{G}^{(i)} = A_{max}^{(i-1)}\mathbf{g}_{max}^{(i)}\mathbf{g}_{max}^{(i)\mathrm{H}} \tag{27}$$

where $\mathbf{g}_{max}^{(i)}$ is the steering vector related to $\mathbf{y}_{max}$. The main objective of this method is to update the dirty map by subtracting a scaled PSF related to $\mathbf{y}_{max}$. This PSF is substituted by a clean beam:

$$Q_j^{(i)} = A_{max}^{(i-1)}\Phi(\mathbf{y}_j - \mathbf{y}_{max}) \tag{28}$$

where Φ is a normalized clean beam ($\Phi(0) = 1$) of specified width. In the following, Φ is chosen as a Dirac Delta function to satisfy this property. The degraded CSM is defined as:

$$\mathbf{D}^{(i)} = \mathbf{D}^{(i-1)} - A_{max}^{(i-1)}\mathbf{g}_{max}^{(i)}\mathbf{g}_{max}^{(i)\mathrm{H}}. \tag{29}$$

The process is then repeated from equation 25. After I iterations, the final source power map at location j is obtained as the summation of the clean beams and the remaining dirty map:

$$A_j = \sum_{i=1}^{I} Q_j^{(i)} + A_j^{(I)} \tag{30}$$

2.6 CLEAN-SC

CLEAN-SC (based on spatial source coherence) has the ability to detect incoherent sources with suitable resolution [15]. The side lobes in a source plot are coherent with the main lobe. The CLEAN-SC method uses this fact to improve the source power map. Physically, this method subtracts all the information which is coherent with the larger mainlobes of the map (strong sources) in order to extract smaller mainlobes (weaker sources) that can be masked by sidelobes of stronger sources. This process is performed iteratively in order to detect all mainlobes (sources) in the source maps. Source cross powers are defined by [15]:

$$A_{jk} = \mathbf{W}_j^{\mathrm{H}}\overline{\mathbf{C}}\mathbf{W}_k \tag{31}$$

where j and k are scan points. Similar to the CLEAN-PSF method, the degraded source powers $A_j^{(i)}$ are obtained by equation 26, but a different matrix $\overline{\mathbf{G}}^{(i)}$ is selected for the CLEAN-SC. Here, $\overline{\mathbf{G}}^{(i)}$ is determined such that the source cross-powers of any scan point $\mathbf{y}_j$ are coherent with the source corresponding to the peak location $\mathbf{y}_{max}$. This means that:

$$\mathbf{W}_j^{\mathrm{H}}\overline{\mathbf{D}}^{(i-1)}\mathbf{W}_{max}^{(i)} = \\ \mathbf{W}_j^{\mathrm{H}}\overline{\mathbf{G}}^{(i)}\mathbf{W}_{max}^{(i)}\text{, for all possible } \mathbf{W}_j, \tag{32}$$

where $\mathbf{W}_{max}^{(i)}$ is the weight vector related to $\mathbf{g}_{max}^{(i)}$. To satisfy equation 32:

$$\overline{\mathbf{D}}^{(i-1)}\mathbf{W}_{max}^{(i)} = \overline{\mathbf{G}}^{(i)}\mathbf{W}_{max}^{(i)} \tag{33}$$

By assuming that $\mathbf{G}^{(i)}$ is due to a single coherent source component $\mathbf{h}^{(i)}$, The solution of equation 33 is:

$$\mathbf{G}^{(i)} = A_{max}^{(i-1)}\mathbf{h}^{(i)}\mathbf{h}^{(i)\mathrm{H}} \tag{34}$$

where $\mathbf{h}$ is a function that represents a distribution of source strengths over grid points.

The trimmed version of equation 34 can be written as:

$$\overline{\mathbf{G}}^{(i)} = A_{max}^{(i-1)}\overline{\mathbf{h}^{(i)}\mathbf{h}^{(i)\mathrm{H}}} = A_{max}^{(i-1)}(\mathbf{h}^{(i)}\mathbf{h}^{(i)\mathrm{H}} - \mathbf{H}^{(i)}) \tag{35}$$

where $\mathbf{H}^{(i)}$ is given by:

$$H_{mn}^{(i)} = \begin{cases} 0 & \text{, for } (m,n) \in S \\ h_m^{(i)}h_n^{(i)*} & \text{, for } (m,n) \notin S \end{cases} \tag{36}$$

As mentioned in equation 7, S is assumed to be a subset of all possibilities of (m,n) combinations, where m and n are microphone indices. To satisfy equation 33, $\mathbf{h}^{(i)}$ must be:

$$\mathbf{h}^{(i)} = \frac{1}{\left(1 + \mathbf{W}_{max}^{(i)\,\mathrm{H}}\mathbf{H}^{(i)}\mathbf{W}_{max}^{(i)}\right)^{1/2}} \\ \cdot \left(\frac{\overline{\mathbf{D}}^{(i-1)}\mathbf{W}_{max}^{(i)}}{A_{max}^{(i-1)}} + \mathbf{H}^{(i)}\mathbf{W}_{max}^{(i)}\right). \tag{37}$$

The expression for $\mathbf{h}^{(i)}$ is not explicit since $\mathbf{H}^{(i)}$ contains (the diagonal) elements of $\mathbf{h}^{(i)}\mathbf{h}^{(i)H}$. However, equation 37 is solved iteratively by starting with $\mathbf{h}^{(i)} = \mathbf{g}_{max}^{(i)}$. After a few iterations equation 37 is usually satisfied. Now a new expression for $\mathbf{G}^{(i)}$ which is different from equation 27 is obtained.

The next steps are exactly identical to the CLEAN-PSF method. The CLEAN-SC is an improved version of the classical clean algorithm. Since the CLEAN-SC does not assume a theoretical beam pattern (PSF), there is better resolution in

the results than that of the classical methods. However, this method can only identify incoherent sources.

2.7 CLEAN-BFR

The basis of the CLEAN-BFR approach is quite similar to the CLEAN-SC. CLEAN-BFR again uses the spatial coherence of sidelobes and mainlobe of a given source in order to identify the sources. Here, all the steps of the CLEAN-SC are repeated but with a weight vector $\mathbf{W}_{\text{BFR}}$ which is obtained from the inverse solution with beamforming regularization. Therefore, source cross powers for CLEAN-BFR are given by [11]:

$$A_{jk} = \mathbf{W}_{\text{BFR}_j}^{\text{H}} \bar{\mathbf{C}} \mathbf{W}_{\text{BFR}_k} \tag{38}$$

where $\mathbf{W}_{\text{BFR}}$ is the weight vector given by equation 20, $\mathbf{W}_{\text{BFR}} = (\mathbf{G}^{\text{H}}\mathbf{G} + \boldsymbol{\epsilon}^2[\text{diag}(|\mathbf{G}^{\text{H}}\mathbf{p}|/\|\mathbf{G}^{\text{H}}\mathbf{p}\|_\infty)^2]^{-1})^{-1}\mathbf{G}^{\text{H}}$. All the subsequent steps of the CLEAN-BFR are identical to CLEAN-SC replacing W by $\mathbf{W}_{\text{BFR}}$.

3 Simulation study

3.1 Sound Field Simulation

The objective of this section is to simulate the sound propagation from simple source models to the microphone array, in order to simulate the various source identification approaches investigated in the previous section. We consider in general two compact sources at locations $\mathbf{r}_1$, $\mathbf{r}_2$ with specific far-field directivity functions $D_1(\theta)$, $D_2(\theta)$ and source magnitudes $q_1(\omega)$, $q_2(\omega)$, such that the sound pressure at the location of microphone m is

$$p_m(\omega) = D_1(\theta)q_1(\omega)\frac{e^{-jk|\mathbf{r}_1-\mathbf{r}_m|}}{|\mathbf{r}_1-\mathbf{r}_m|} + \\ D_2(\theta)q_2(\omega)\frac{e^{-jk|\mathbf{r}_2-\mathbf{r}_m|}}{|\mathbf{r}_2-\mathbf{r}_m|}. \tag{39}$$

The case of monopoles, dipoles and quadrupoles radiating in the far-field will be considered. A dipole is represented by two closely spaced monopoles of magnitudes $-q_i(\omega), +q_i(\omega)$ with a separation d (such that $kd \ll 1$) [24]. For a dipole at location $\mathbf{r}$, the sound pressure at the location of microphone m is:

$$p_m(\omega) = kd\cos\theta\, q_i(\omega)\frac{e^{-jk|\mathbf{r}-\mathbf{r}_m|}}{|\mathbf{r}-\mathbf{r}_m|} \tag{40}$$

Here, the directivity is $D_i(\theta) = \cos\theta$ where θ is the angle relative to the dipole axis and the dipole magnitude is given by $q_{dip,i}(\omega) = jkdq_i(\omega)$ where $= |\mathbf{k}|$.

A tesseral quadrupole is represented by four closely spaced monopoles of magnitudes $+q_i(\omega), -q_i(\omega), -q_i(\omega), +q_i(\omega)$ with separations d along the two orthogonal axes (such that $kd \ll 1$). For a quadrupole, $D_i(\theta) = \cos\theta\sin\theta$ and the quadrupole magnitude is given by $q_{quad,i}(\omega) = -k^2d^2q_i(\omega)$ [24].

The cross-spectral power of sound pressures at two distinct locations ($\mathbf{r}_m$ and $\mathbf{r}_n$) is given by:

$$\begin{aligned} C_{nm} \\ = p_n^* p_m = \; & D_1(\theta)^2 S_{11}\frac{e^{jk(|\mathbf{r}_1-\mathbf{r}_n|-|\mathbf{r}_1-\mathbf{r}_m|)}}{|\mathbf{r}_1-\mathbf{r}_m||\mathbf{r}_1-\mathbf{r}_n|} \\ & + D_2(\theta)^2 S_{22}\frac{e^{jk(|\mathbf{r}_2-\mathbf{r}_n|-|\mathbf{r}_2-\mathbf{r}_m|)}}{|\mathbf{r}_2-\mathbf{r}_m||\mathbf{r}_2-\mathbf{r}_n|} \\ & + D_1(\theta)D_2(\theta)S_{12}\frac{e^{jk(|\mathbf{r}_2-\mathbf{r}_n|-|\mathbf{r}_1-\mathbf{r}_m|)}}{|\mathbf{r}_2-\mathbf{r}_n||\mathbf{r}_1-\mathbf{r}_m|} \\ & + D_1(\theta)D_2(\theta)S_{12}^*\frac{e^{jk(|\mathbf{r}_1-\mathbf{r}_n|-|\mathbf{r}_2-\mathbf{r}_m|)}}{|\mathbf{r}_1-\mathbf{r}_n||\mathbf{r}_2-\mathbf{r}_m|} \end{aligned} \tag{41}$$

where $S_{11} = q_1(\omega)q_1^*(\omega)$, $S_{22} = q_2(\omega)q_2^*(\omega)$ are the auto-spectral power densities of the two sources and $S_{12} = q_1(\omega)q_2^*(\omega)$ is their cross-spectral power density. The value of S_{12} relative to S_{11} and S_{22} allows simulating coherent, incoherent or partially coherent sources. The cross spectral matrix $\mathbf{C}$ is the input of phased array techniques which are applied is this study, and the output is the source power map. Equations 39 and 40 can be easily expanded to more than two sources. The source properties can be defined by changing the source directivity and the correlation parameters of source spectral densities (S_{11}, S_{22} and S_{12}).

3.2 Simulation of source identification methods

In this section, the various source identification algorithms detailed in section 3 are tested through simulations. A regular circular array configuration of 60 microphones on a circle with radius $R = 45$m is considered for the various methods and for different source types. In the following, source power maps are plotted as a function of positions normalized to the acoustic wavelength λ. The scan zone for the simulation study is a rectangular area where $-2\lambda < x < 2\lambda$, $-2\lambda < y < 2\lambda$ and the resolution is 0.1λ The microphone array radius is $R = 132\,\lambda$ (See Figure 1)
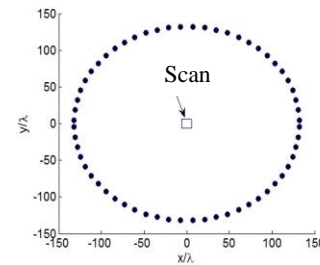
Figure 1: Microphone array configuration

In the situations considered in the following, sources are inside the array and close to the array center. These conditions are similar to the configuration used for static aero-engine noise certification tests (using a semi-circular microphone array) [10].

Figure 2 show the results of conventional beamforming for 1800 microphones, $\frac{d}{\lambda} = 0.45$ (Left) and 60 microphones, $\frac{d}{\lambda} = 14.01$ (Right). The results show the microphones seperation regardless of spatial aliasing condition, in the particular situation of sources close to array center does not essential effect in the map resolution. This aspect needs more investigations.
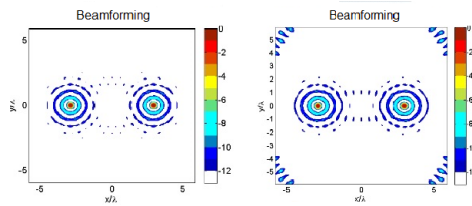
Figure 2: Conventional beamforming output for 1800 microphones and 60 microphones

Identification of sources with unequal amplitude

The application of the approaches for sources with unequal strengths is investigated. Two uncorrelated monopole sources at positions $\frac{x}{\lambda} = -1, +1$ with a 6dB difference in source powers are considered ($S_{11} = 1[\text{kg}^2\text{s}^{-4}]$, $S_{22} = 4[\text{kg}^2\text{s}^{-4}]$, $S_{12} = 0[\text{kg}^2\text{s}^{-4}]$).

Figure 3 shows the source power maps of two uncorrelated monopoles in dB relative to the peak value for the different methods. The plot range in this figure is 12 dB, which is almost the same as the dynamic range (peak level minus highest side lobe level) of the microphone array that was used. In the results, ϵ is the regularization parameter and it is the number of iterations in L1-GIB, CLEAN-PSF, CLEAN-SC and CLEAN-BFR. It can be observed that conventional beamforming and the regularized inverse method are able to correctly identify the relative amplitude values and the location of the sources. However, both methods display strong sidelobes that can potentially mask weaker sources. The BFR method is not able to determine the weaker sources because of the large penalization being applied to a weaker source (see equation 13), resulting in an underestimation of source strength for this source. CLEAN-PSF, CLEAN-SC, L1- GIB and CLEAN-BFR provide high resolution maps. The dB value of the weaker source is shown in figure 3 for all the methods.

Identification of Correlated and Uncorrelated Sources

Identification algorithms are applied for uncorrelated ($S_{11} = 1[\text{kg}^2\text{s}^{-4}]$, $S_{22} = 1[\text{kg}^2\text{s}^{-4}]$, $S_{12} = 0[\text{kg}^2\text{s}^{-4}]$), correlated ($S_{11} = 1[\text{kg}^2\text{s}^{-4}]$, $S_{22} = 1[\text{kg}^2\text{s}^{-4}]$, $S_{12} = 1[\text{kg}^2\text{s}^{-4}]$) and partially correlated sources ($S_{11} = 1[\text{kg}^2\text{s}^{-4}]$, $S_{22} = 1[\text{kg}^2\text{s}^{-4}]$, $S_{12} = 0.25[\text{kg}^2\text{s}^{-4}]$) (See Figure 4).

The CLEAN-SC and CLEAN-BFR methods detect partially correlated sources as well as uncorrelated sources. However, these methods do not satisfactorily detect correlated sources.
In the first iteration of these algorithms, the mainlobe of the strongest source and all coherent parts in the source power map will be removed. Accordingly, weaker sources that are coherent with the mainlobe will also be removed. This reveals that the CLEAN-SC and the CLEAN-BFR are inappropriate for coherent sources. BFR and L1-GIB show consistent results for uncorrelated sources as well as correlated and partially correlated sources
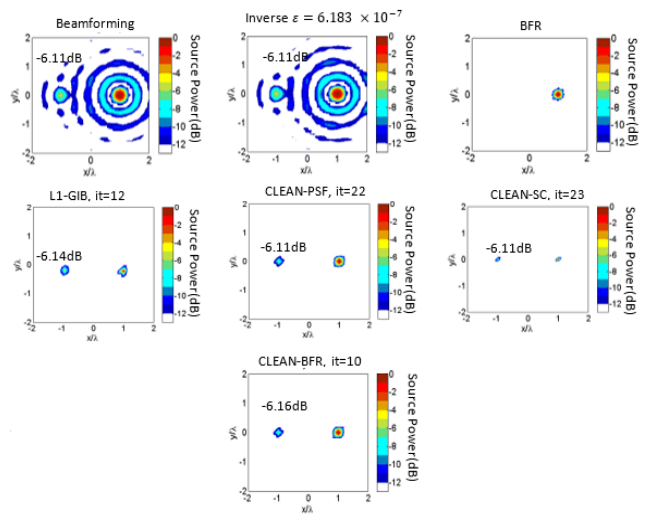
Figure 3: Source power maps for two uncorrelated monopoles in dB relative to the peak value for the different methods (with a 6dB level difference)

3.3 Identification of monopole, Dipole and Quadrupole Sources

In this section, the methods are tested for multipole source identification. For both dipole and quadruple sources, $kd = 0.369$ (see section 3.1). The sources are uncorrelated and are positioned on $[\lambda, 0]$ and $[-\lambda, 0]$. Both dipole and quadrupole sources are parallel to the array plane. As seen in Figure 5, the dipole source is oriented along the x-axis and two intensity peaks are on the source maps that the central point between the peaks corresponds to the dipole position ($\frac{x}{\lambda} = +1, \frac{y}{\lambda} = 0$). The crosses in the figure represent actual source positions. The quadrupole is considered as four monopoles (see section 3.1). The Four intensity peaks are seen on the source maps that the central point among the peaks corresponds to the quaropole position($\frac{x}{\lambda} = -1, \frac{y}{\lambda} = 0$).

The auto-spectral power densities (S_{qq}) of the monopole source is equal to $1[\text{kg}^2\text{s}^{-4}]$. The dipole source consists of two monopole sources with $S_{qq} = 4[\text{kg}^2\text{s}^{-4}]$ and the quadrupole source consists of four monopole sources with $S_{qq} = 16[\text{kg}^2\text{s}^{-4}]$.

As shown in Figure 5 all algorithms can identify uncorrelated monopole, dipole and quadrupole sources. However, the best results are provided by BFR, L1-GIB, CLEAN-SC and CLEAN-BFR.
Table 1 compares the different methods in various aspects. The check mark (✓) indicates the concept "yes" and the ✗ mark is used to indicate "no". It is obvious that BFR, CLEAN-PSF, CLEAN-SC, L1- GIB and CLEAN-BFR provide higher resolution maps compared to conventional beamforming and the regularized inverse. Choosing one of these methods as the best method entirely depends on the problem's circumstances and the type of sound sources.
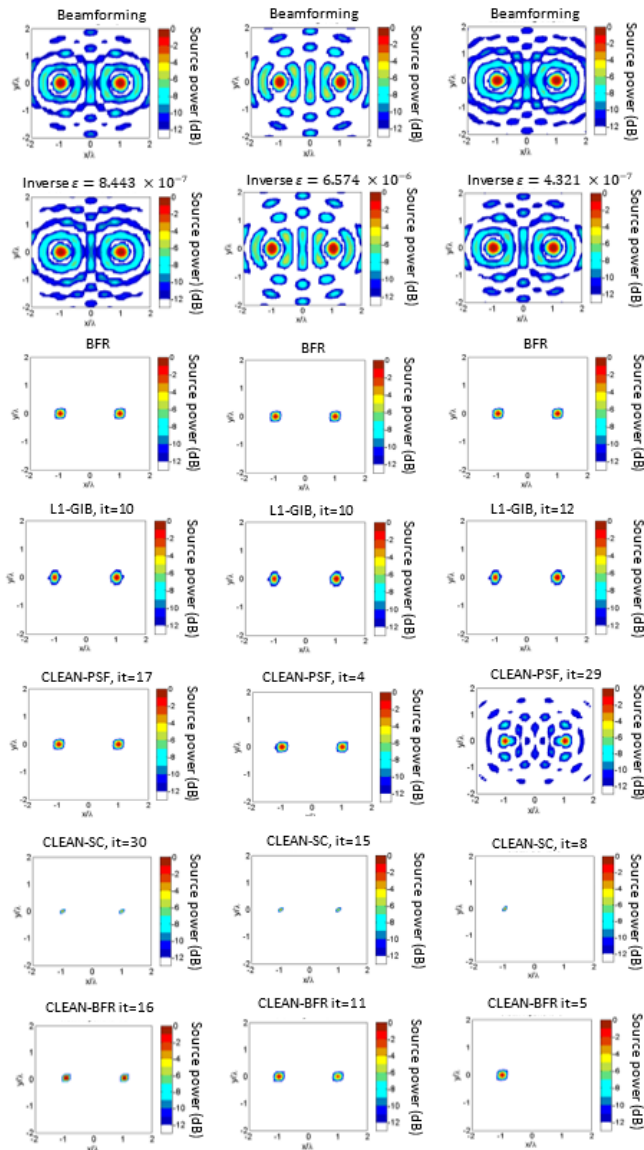
Figure 4: Source power maps for the various methods: Left: Two uncorrelated monopoles, Center: Two partially correlated monopoles, Right: Two fully correlated monopoles

4 Experiment

The laboratory test set-up designed to validate the source identification approaches uses two Audiophile DX4 satellite loudspeakers placed back-to-back on the floor of the Sherbrooke university hemi-anechoïc chamber (Figure 6). Each loudspeaker was fed independently with a broadband input. Loudspeakers were moved along the red line in figure 4 to validate the application of the various approaches for different source locations.

The measurements were provided by a 1.78 m radius semi-circular array of B&K4189 ½ inch free-field microphones installed on the ground. Although the anticipated application is for far-field, outdoor microphones and noise source separation of aero-engines, a small microphone antenna was tested in laboratory to validate the results of simulations.
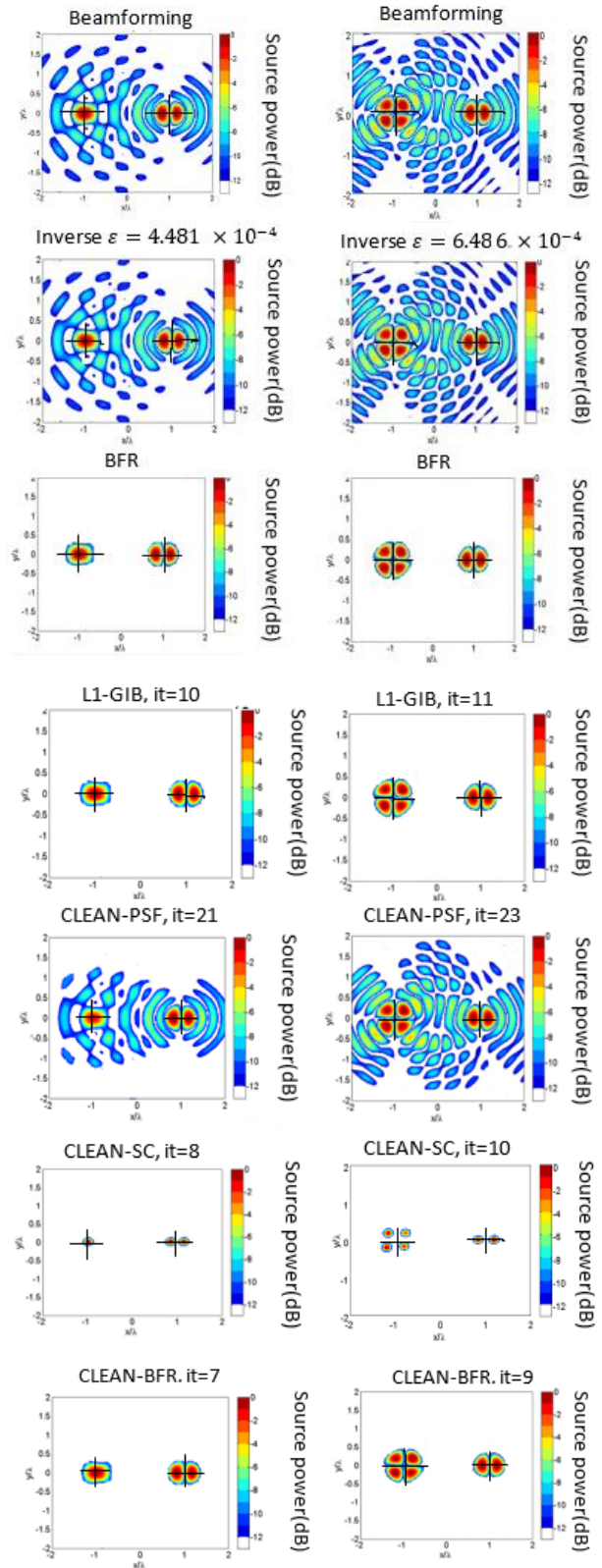
Figure 5: Source power maps for monopole, dipole and quadrupole sources:(left) one monopole and one dipole source (Right) one quadrupole and one dipole source

Figure 6: Experimental set-up in the laboratory

The semi-circular array has 94 microphones, with a microphone separation of approximately 6 cm. A second semi-circular array of microphones is virtually created by assuming axi-symmetry of the sound radiation from the loudspeakers with respect to the axis-line (red line in Figure 6). This configuration has the advantage of virtually increasing the number of sound pressure data and array aperture without implying additional physical measurements. The presence of a hard ground in the experiments induces pressure doubling at the microphones with respect to a free-field situation. Since only normalized source power maps are presented, no special modification of microphone signals was carried to account for the reflective ground surface. Microphone signals were acquired on a Bruel&Kjaer Pulse system. Then, the cross spectral matrix of microphone signals was built. The loudspeaker inputs were Gaussian noise in the frequency range from 0 to 12,000Hz. The scan zone is in the plane of microphones, and for all tests is $-1.4\text{m} < x < 1.4\text{m}$ and $-1.4\text{m} < y < 1.4\text{m}$, and the scan grid resolution is 0.02m.

Three source configurations were tested:

1- Two loudspeakers driven by uncorrelated broadband inputs with the same amplitude, at positions (0.3 m, 0) and - 0.3 m, 0)

2- Two loudspeakers driven by uncorrelated broadband inputs with 7dB difference in amplitudes, at positions (0.75 m, 0) and (-0.75 m, 0)

3- Two loudspeakers driven with the same Gaussian white noise, at positions (0.75 m, 0) and (-0.75 m, 0)

Figure 7 shows the source power maps for the two uncorrelated loudspeakers with identical amplitudes at positions (0.3 m, 0) and (- 0.3 m, 0) at $f = 1$ kHz. The crosses in the figures represent actual loudspeaker positions (position of front face). As shown in figure -7 most approaches correctly detect the source positions and relative magnitudes. However, conventional beamforming and the regularized inverse method display many sidelobes like for numerical simulations. Although the CLEAN-PSF partially removes side lobes, it still does not satisfy expectations of a source power map with high resolution. The L1-GIB results show that while source distances are decreased, the performance of L1-GIB drops (compare L1-GIB results in figures 8 and9).

The best results are provided by the CLEAN-SC, the CLEAN-BFR and the BFR methods. This conclusion is consistent with the simulation results of section 3.

Figure 8 shows results at $f = 1$ kHz for two uncorrelated broadband sources with 7 dB level difference. The two speakers are set up at (0.75 m, 0) and (-0.75 m,0). The measured power of the weak source relative to the strong source is provided in the figure.
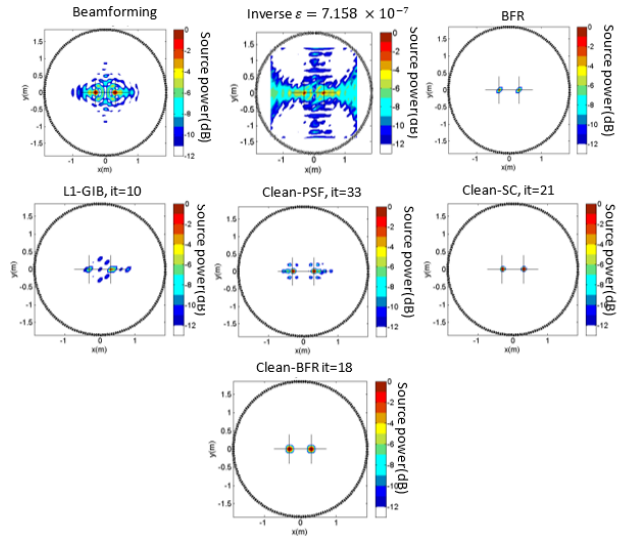
Figure 7: Source power maps for two loudspeakers driven by uncorrelated inputs with the same amplitude, at positions (0.3 m, 0) and - 0.3 m,0) at $f = 1$ kHz. (The circle is the microphone array)
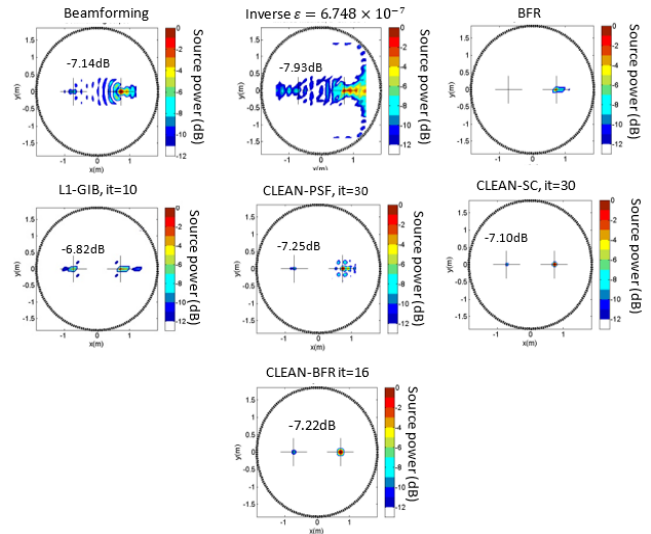
Figure -8: Source power maps,for two loudspeakers driven by uncorrelated inputs with 7 dB level difference, at positions (0.75 m,0) and (-0.75 m, 0) at $f = 1$ kHz. (The circle is the microphone array)

All methods correctly detect the sound radiation from the strongest source. However, due to strong sidelobes, conventional beamforming and the inverse method cannot detect the weaker source with enough resolution. The BFR method, as shown in the simulation section, is unable to detect weaker sources in the presence of the strong sources. This is due to the largest penalization being applied to a weaker source in
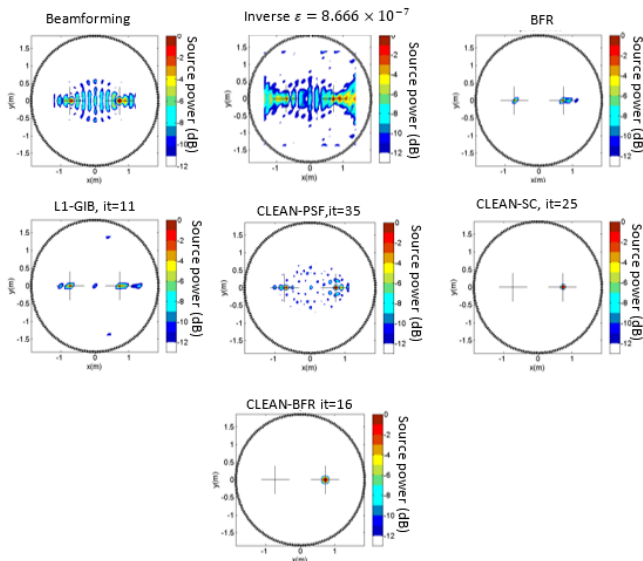
Figure -9: Source power maps for two loudspeakers driven by correlated inputs with 7 dB level difference, at positions (0.75 m,0) and (-0.75 m,0) at $f = 1$ kHz. (The circle is the microphone array)

the BFR method (see equation 19), which results in the underestimation of source strength for this source. Similar to the simulation study, the CLEAN-SC and the CLEAN-BFR provide the best results.

In the last experiment, the two loudspeakers are driven by the same Gaussian white noise signal. The two sources are therefore perfectly correlated. As seen in figure 9, the results indicate that similar to the simulation results, source correlation is not a significant parameter for conventional beamforming, the regularized inverse method, the BFR method and the L1-GIB. The CLEAN-PSF improves the resolution of source maps. As mentioned in the simulation section, the CLEAN-SC and CLEAN-BFR methods are based on the idea that sources in source plots are spatially coherent with their sidelobes. Therefore, for two correlated sources, one of the sources is identified as a coherent sidelobe of the other source and is therefore automatically removed from the map

after the first iteration. The CLEAN-SC and the CLEAN-BFR are therefore not applicable for coherent sources. Overall, the BFR method provides the best results for two coherent sources.

5   Conclusion

This paper has examined the use of a circular microphone arrays to identify noise sources near the array center. An important application is for separation of exhaust / inlet noise of aero-engines using far-field circular microphone antenna. To this end, established methods have been tested (conventional beamforming, regularized inverse approach, CLEAN-PSF, CLEAN-SC, L1-GIB) as well as well more recent approaches (Beamforming Regularization Method, BFR). A new method (CLEAN-BFR) combining the iterative concepts of CLEAN-SC and BFR has been proposed. The findings of numerical simulations have been validated through laboratory experiments using a small antenna.

The principal conclusions are:

- BFR, CLEAN-PSF, CLEAN-SC, L1- GIB and CLEAN-BFR provide higher resolution maps compared to conventional beamforming and the regularized inverse.
- For sources with unequal magnitudes, the BFR method is not able to determine the weaker sources because of the large penalization applied to this weaker source, resulting in an underestimation of source strength for this source.
- CLEAN-SC and CLEAN-BFR are inappropriate for coherent sources
- BFR, L1-GIB, CLEAN-SC and CLEAN-BFR perform effectively for uncorrelated, dipole or quadrupole sources.

Acknowledgments

Table 1: Comparison of the sound identification methods in various aspects

Methods	High resolution	Identification of various types of sound sources				Rank of methods based on computation time
		Multipole sources	Correlated sources	Uncorrelated sources	Sources with different amplitudes	
Beamforming	✗	✓	✓	✓	✓	1
Inverse	✗	✓	✓	✓	✓	2
BFR	✓	✓	✓	✓	✗	3
L1-GIB	✓	✓	✓	✓	✓	6
CLEAN-SC	✓	✓	✗	✓	✓	7
CLEAN-PSF	✗	✓	✓	✓	✓	5
CLEAN-BRF	✓	✓	✗	✓	✓	4

References

[1] T. Padois,A. Berry, and P.-A. Gauthier,Beamforming matrix regularization and inverse problem for sound source localization: Application to aero-engine noise, *19th AIAA/CEAS Aeroacoustics Conference,*2013

[2] P. Sijtsma, Feasibility of noise source location by phased array beamforming in engine ducts, *Aeroacoustics Conference*, Rome, 21-23, 2007.

[3] T. Bravo, and C. Maury, Microphone array beamforming and inverse methods for the reconstruction of ducted acoustic sources, *14th International Congress on Sound and Vibration (ICSV14)*, Australia, 2007.

[4] U. Michel, D. Zentrum, and F. Luft, History of acoustic beamfomring, *Berlin Beamforming Conference (BeBeC),* 2006.

[5 U. Michel, and S. Funke, Inverse method for the acoustic source analysis of an aeroengine, *Berlin Beamforming Conference (BeBeC)*, 2008.

[6] S.H. Yoon, and P.A. Nelson, Estimation of acoustics source strength by inverse method: Part II, experimental investigation of methods for choosing regularization parameters, *J. Sound and Vibr*, 233:4, 2000.

[7] E. Sarradj, A fast signal subspace approach for the determination of absolute levels from phased microphone array measurements, *J. Sound and Vibr*, 329:9, 2000.

[8] P.A.G. Zavala, W. De Roeck, K. Janssens, J.R.F. Arruda, P. Sas, and W. Desmet, Generalized inverse beamforming investigation and hybrid estimation, *Berlin Beamforming Conference (BeBeC)*, 2010.

[9] T. Padois, P.A. Gauthier, and A. Berry,Inverse problem with beamforming regularization matrix applied to sound source localization in closed wind-tunnel using microphone array, *J. Sound and Vibr*, 333:25, 2014.

[10] I. Khatami, and A. Berry, Source localization of aircraft engines with circular microphone arrays, Canadian Acoustics Conference, 39:3, 2011.

[11] I. Khatami, A. Berry, N. Joshi, and S.A. Meslioui, Source identification of a gas turbine engine using an inverse method with beamforming matrix regularization, *Berlin Beamforming Conference (BeBeC),* 2012.

[12] P.Chiariotti , M.Martarelli , and P. Castellini,Acoustic beamforming for noise source localization – Reviews,methodology and applications, *Mechanical Systems and Signal Processing* ,2019

[13] R.O. Schmidt, Multiple emitter location and signal parameter estimation, *IEEE Transactions on Antennas and Propagation*, 34:3, 1986.

[14] R. Roy, A. Paulraj, and T. Kailath, ESPRIT: a subspace rotation approach to estimation of parameters of cisoids in noise, *IEEE Transactions on Acoustics, Speech and Signal Processing*, 34:5, 1986.

[15] P. Sijtsma, CLEAN based on spatial source coherence, *AIAA paper*, 6:4, 2007.

[16] T.F. Brooks and W.M. Humphreys, A deconvolution approach for the mapping of acoustic sources (DAMAS) determined from phased microphone arrays, *J. Sound and Vibr*, 294:4-5, 2006.

[17] Q.Lecle`re, A.Pereira,C.Bailly,J.Antoni1 and C Picard, A unified formalism for acoustic imaging based on microphone array measurements*, International Journal of Aeroacoustics*,2017

[18] T. Suzuki, Generalized beamforming algorithm resolving coherent/incoherent distributed and multipole sources, *14th AIAA/CEAS Aeroacoustics conference (29th AIAA Aeroacoustics conference)*, 2008.

[19] T. Suzuki, L_1 generalized inverse beam-forming algorithm resolving coherent/incoherent, distributed and multipole sources, *J. Sound and Vibr*, 330:24, 2011.

[20] Brüel&Kjær, Technical review beamforming,[Report], 2004.

[21] Dougherty R. P. What is beamforming, *Berlin Beamforming conference (BeBeC)*, 2008.

[22] C. Hansen ,Rank-Deficient and Ill-Posed Problems, *Philadelphia: SIAM*, 1998.

[23] P.J. Huber, Robust Statistics**,** Wiley Series in Probability and Statistics, *John Wiley & Sons*, 1981.

[24], M. Bruneau, Introduction aux théories de l'acoustique, *Publications de l'université du Maine*, 1993.